Phys. Status Solidi A **213**, No. 11, 2809–2819 (2016) / **DOI** 10.1002/pssa.201600713

physica status solidi a
www.pss-a.com
applications and materials science

Feature Article

Strained germanium for applications in spintronics

Christopher Morrison and Maksym Myronov*

Department of Physics, The University of Warwick, Coventry CV4 7AL, UK

Received 8 August 2016, revised 26 September 2016, accepted 26 September 2016
Published online 7 November 2016

Keywords germanium, Rashba spin–orbit interaction, spintronics

* Corresponding author: e-mail: m.myronov@warwick.ac.uk, Phone: +44 (0)24 765 74383, Fax: +44 (0)24 765 74383

Germanium (Ge) is another group-IV semiconductor material, which recently started attracting tremendous attention in spintronics following success of silicon (Si). The crystal inversion symmetry of Si and Ge precludes the spin relaxation of conduction electrons by the Dyakonov–Perel mechanism, resulting in a long spin relaxation time. Since the proposal of the spin FET in 1990 by Datta and Das, semiconductor materials have been studied for their spin–orbit (S–O) interactions, particularly those that can be modified by an applied electric field, such as the Rashba S–O interaction, in order to create devices that utilise spin modulation and control to perform logic operations. Since then new proposals have appeared. Nowadays they include spin transistors with several different operating principles, spin-based diodes, spin-based field programmable gate arrays, dynamic spin-logic circuits, spin-only logic, spin communication and others. In this review, the focus will be made on presenting recent progress in Ge spintronics including the key advances made. The absence of Dresselhaus S–O coupling in Ge enables a longer spin diffusion length when compared to III–V semiconductor materials. Evidence of a strong Rashba S–O interaction in strained Ge quantum wells has begun to emerge. Also, the first experimental demonstration of room-temperature spin transport in Ge has recently been reported.

© 2016 WILEY-VCH Verlag GmbH & Co. KGaA, Weinheim

1 Introduction

Spintronics is a study of the intrinsic spin of the electron or hole and its associated magnetic moment in solids (see Fig. 1). Electrons or holes have ½ spin which can be either up or down. Spintronics promises lower energy consumption compared to traditional electronics because charge interaction energy scale is eV and the spin interaction energy scale is meV. When a magnetic field is applied to a magnetic moment, the moment experiences a torque to try to align the moment with the field to minimise energy. As the magnetic moment of an electron is proportional to its angular momentum, the torque applies a change in angular momentum perpendicular to the initial state. The magnetic field thus causes the spin to precess about the field and can, therefore, be used to modulate spin (see Fig. 1). Spintronics has had, and continues to have, a significant impact on technological applications [1]. Uncertainty in the prospects of future generations of electronic devices based on charge transport, manipulation and storage has led to rapid research into alternative technologies. Power consumption and heat generation are the most significant limiting factors in modern and future electronic device architectures. Scaling of classical metal oxide semiconductor field effect transistor (MOSFET), diodes and other devices faces extraordinary challenges and has already resulted in dramatic changes in their designs including transformation of the most advanced electronic devices from 2D to a 3D architecture. For these reasons, alternative technologies are increasingly desired as a supplement to or complete replacement of conventional complimentary metal-oxide semiconductor (CMOS) devices. This focus is reflected in the International Technology Roadmap for Semiconductors which targets emerging technologies, one of which is spintronics. A significant advantage of spintronic devices is the potential for reduced energy consumption. Indeed, both the power consumption and the speed of spintronic computing can be comparable to charge electronic devices scaled to the limit of operation and fabrication capability. Beyond these implementations of spintronics, the possibility of using a completely dissipation-less spin current would provide even greater technological rewards. The clear aim for modern spintronics research is to produce an energy efficient, fast alternative for computational and memory applications.

© 2016 WILEY-VCH Verlag GmbH & Co. KGaA, Weinheim

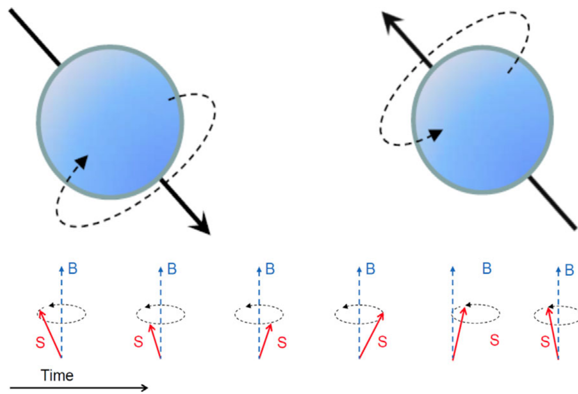

Figure 1 Electrons have ½ spin which can be either up or down. When a magnetic field is applied to a magnetic moment, the moment experiences a torque to try to align the moment with the field to minimise energy. The magnetic field causes the spin to precess about the field and can therefore be used to modulate spin.

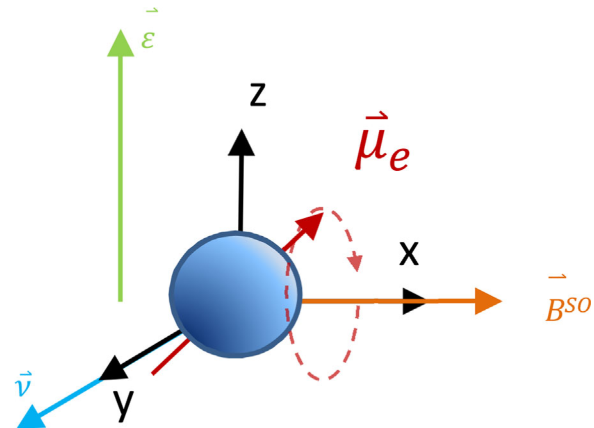

Figure 2 A visualisation of the Rashba spin–orbit interaction on mobile carriers in a semiconductor. The spin magnetic moment μ_e of a charge carrier with velocity v precesses about the spin–orbit magnetic field B_{SO} induced by an electric field ε.

A further stimulus comes from proposals of new concepts for electronic devices and circuits that use spin orientation to encode binary information. Spintronic devices based on metallic elements have been extremely successful, seeing multiple applications in areas such as magnetic data storage (hard disk read heads) and non-volatile random access memory (magnetic random access memory (MRAM)).

In semiconductor spintronics, most research is focused upon integration of semiconductors and magnetic materials, aiming to create an energy efficient information technology in which digital data are encoded in the spin of electrons or holes. Implementing spin functionality in mainstream semiconductor materials such as silicon (Si) or materials epitaxially grown on a silicon substrate is essential to establish a spin-based electronics, and possibly photonics, with the potential to change information technology and the world around us beyond imagination. Germanium (Ge), due to its superior spin properties, is one of those materials and the main rival for silicon.

2 Si and III–V spintronics The spin diffusion length is a key parameter to describe the transport properties of spin polarised electrons in solids and defines a length over which the spin of the electron preserves the memory of its initial orientation [2, 3]. Electrical spin injection in semiconductor structures is a major issue in spintronics, and it strongly depends on the spin diffusion length. In semiconductors, this distance is tightly linked to spin relaxation and the spin transport properties of conduction electrons or holes. Also it depends on the spin–orbit interaction (SOI) [2, 3]. In quantum wells (QW) made of III–V semiconductors, such as GaAs the conduction-band spin splitting has two origins: the first one, called bulk inversion asymmetry (BIA) or Dresselhaus term, is the consequence of the combined effect of SOI and the lack of crystal inversion symmetry [2, 3]. The second contribution to the spin splitting, called structural inversion asymmetry (SIA) or Rashba term, exists if the QW or channel experiences an electric field [4]. A visualisation of the Rashba SOI on mobile carriers in a semiconductor is depicted in Fig. 2.

Efforts to create spin polarisation in semiconductors by electrical means, known as electrical spin injection, were initiated after the first proposal of a spin transistor [5]. The transistor relied on SOI, making III–V materials with strong spin–orbit coupling, such as InAs, favourable. Moreover, optical methods using luminescence in a III–V light-emitting diode (LED) provided a convenient means to detect and prove the presence of the electrically induced spin polarisation, and to quantify it. Both factors secured the dominance of III–V materials. The first electrical spin injection was achieved at room temperature in III–V semiconductor devices. All these advances have been described extensively in the existing literature [6].

Much of the early work in group-IV semiconductor spintronics focused on spin injection into silicon. Spin injection into silicon was first achieved in 2006, using tunnel contacts with an Al_2O_3 barrier [7]. In 2009, room temperature spin injection was achieved in heavily n- and p-doped silicon [8]. Since these milestones, many similar studies have been performed and these are summarised elsewhere [1]. A common parameter determined both electrically and optically is the spin lifetime and the related spin diffusion length. These parameters are the characteristic time/length over which an accumulated carrier spin polarisation decays within the semiconductor. These parameters are, therefore, important for device applications as they define the length scale over which spin information can be transmitted with negligible loss of spin polarisation. The largest spin lifetimes observed in Si using electrical (Hanle) techniques and electron spin resonance (ESR) are summarised in Table 1.

As a result of the initial research on the ability of electrons or holes to exhibit one of two states of spin, known

© 2016 WILEY-VCH Verlag GmbH & Co. KGaA, Weinheim

Table 1 Spin lifetimes in Si at low- and room-temperature. Spin lifetime is carrier density dependent; the largest value is given in the table (for the lowest carrier density). Typical carrier densities are in the range of 10^{18}–10^{20} cm^{-3}. Spin lifetimes determined by three terminal (3T) Hanle, non-local (4T) Hanle and electron spin resonance (ESR) are listed.

temperature (K)	dopant type	spin lifetime (3T Hanle) (ns) [8, 9]	spin lifetime (non-local Hanle) (ns) [10]	spin lifetime (ESR) (ns) [11–13]
10	n	0.3	10	300
300	n	0.3	1	8.5
300	p	0.27	–	–

as spin up and spin down, led to appearance of the spin field effect transistor (spin FET) proposal. A schematic of the spin FET design, proposed by Datta and Das [5] is shown in Fig. 3. Spin polarised carriers are injected at the source, and under zero applied gate voltage they diffuse to the drain, where they are extracted through the ferromagnetic contact. When a gate voltage is applied, the spin of carriers in the channel are rotated under the action of the Rashba spin–orbit field. The geometry of the device is such that the spin rotates to the opposite direction with respect to the injected carriers, as a result a large degree of spin scattering occurs at the drain, resulting in a high resistance state. Therefore, a similar operation to a conventional transistor (invented in the 1940s) is obtained.

3 Ge spintronics Interest in spintronics utilising Ge has greatly increased in recent years. Our ability to generate, detect and manipulate the spin will lead to creation of spin logic and memory devices based on Ge (Fig. 4). Ge has an intrinsic SOI, and through formation of QW heterostructures the Rashba interaction arises through SIA. This allows for control of spin transport via an applied electric field through, for example, a gate. As Ge has a centrosymmetric, diamond cubic crystal structure, and is an elemental semiconductor,

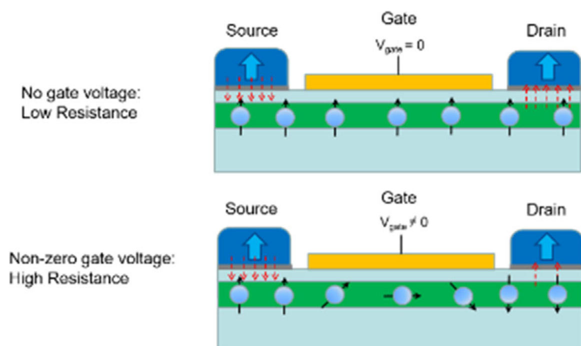

Figure 3 Proposed spin field effect transistor (Spin FET) device, after Datta and Das [5].

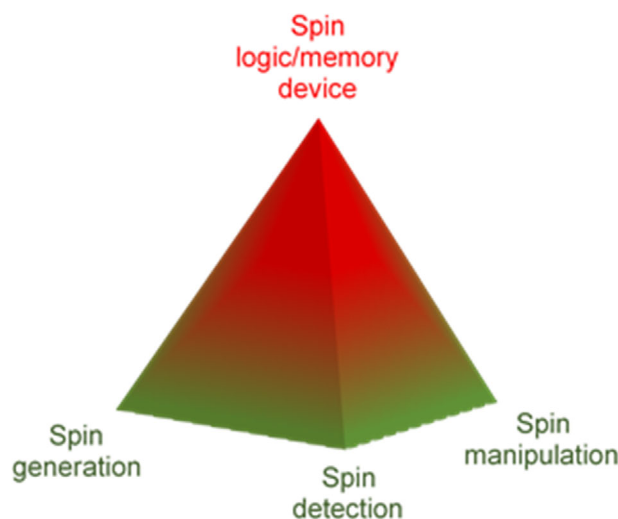

Figure 4 The cornerstones of germanium spintronics, the generation, manipulation and detection of spin polarisation. They are essential to create spin logic and memory Ge devices.

there is no Dresselhaus spin–orbit term that would arise from BIA. This is advantageous as the Dresselhaus interaction is a constant term and cannot be tuned by an external electric field. Holes in a strained Ge 2D hole gas (2DHG) are confined in the heavy hole band, and as such afford an excellent opportunity to study the cubic Rashba interaction, as opposed to the linear effect seen in electron and light hole systems. Spin lifetimes in Ge have been found to be relatively long, up to 0.5 ns [14] at room temperature and a spin diffusion length of up to ~660 nm [15]. Strain in a Ge epilayer or QW can be tuned by growth onto a silicon germanium (SiGe) relaxed buffer layer, the magnitude of the strain is tuned through the Ge composition of the buffer. Strain changes the mobility of carriers in Ge, with the highest mobilities to date found in Ge layers grown on an ~70–80% Ge SiGe buffer layer [16–18]. Ge is highly compatible with conventional Si-based technology, and can be grown with high material and electrical quality onto standard orientation silicon substrates. Thus, it is possible for Ge-based spin transport field effect transistors with small gate lengths to overcome the scaling limits of Si-based devices. Additionally, in recent years, significant success has been achieved in the thermal growth of a high quality germanium dioxide (GeO_2) dielectric layer with a gate function in the Ge-based metal oxide semiconductor field effect transistor [19]. The GeO_2 exhibits a low interfacial density of states to the bulk Ge, allowing for formation of high quality gates for control of spin and charge transport. Moreover, spin injection and spin relaxation in Ge have been extensively studied using electron spin resonance [20–25] and optical techniques [26–29]. However, in spite of all the recent progress in the Ge field and in contrast to Si, spin transport in Ge using nonlocal four-terminal techniques has only been observed at low temperatures to date [30–32]. Spin transport has been reported through a Ni/Ge/AlGaAs

 © 2016 WILEY-VCH Verlag GmbH & Co. KGaA, Weinheim

junction; however, optical spin injection lacks the scalability needed for nanoelectronic applications [33]. Some electrical studies [31, 34, 35] reported spin injection into highly doped n-Ge at room temperature (RT), raising the possibility that RT Ge spintronics can be realised. Unfortunately, these studies used a three-terminal method, the reliability of which is now being called into question. Many recent studies demonstrated that signals in the three terminal geometry originate not from spin accumulation in nonmagnetic channels but from magnetic field-dependent tunnelling through localised states [36–42] Other studies revealed that ferromagnetic NiFe, commonly used as a contact material, itself generates electromotive forces by the inverse spin-Hall effect (ISHE) [43] and the planar Hall effect [44]. Careful control experiments are indispensable to eliminate the self-induced electromotive forces from NiFe. Just recently, realisation of RT spin transport in Ge was demonstrated which was long awaited for further progress in semiconductor spintronics [15]. By utilising spin pumping under ferromagnetic resonance a pure spin current was generated in the n-Ge at room temperature. The pure spin current was detected by using the inverse spin-Hall effect of either a Pt or Pd electrode on n-Ge. The spin diffusion length in n-Ge at RT was estimated to be 660 nm. Moreover, the spin relaxation time decreases with increasing temperature, in agreement with a recently proposed theory of donor-driven spin relaxation in multivalley semiconductors.

4 Spin properties of bulk Ge Progress in Ge has been slower than in silicon, in part due to the relative scarcity of high quality Ge wafers for research. Spin injection into n-type Ge at RT was first realised in 2010, using optical spin excitation and detection [33]. All electrical spin injection, transport and detection was first achieved in the following year [32], although only at temperatures up to 225 K. RT spin transport was achieved in 2015, using spin pumping by ferromagnetic resonance of a permalloy electrode to achieve spin injection [15]. Optical techniques have also been used for spin injection, transport and detection at RT [48, 49]. While spin injection and transport in p-type Ge has been observed at low temperatures, albeit by a combination of techniques and not in a single spintronic device [47]. this has not been achieved at RT to date. These key milestones are summarised in the timeline shown in Fig. 5. Spin lifetimes and spin diffusion lengths measured for n- and p-type Ge using local and non-local Hanle measurements are summarised in Table 2.

Although the electronic properties of Ge are superior to those of Si, Ge wafers are heavier, less durable and much more expensive than their Si analogy (Table 3) Thus, it is desirable to combine the superior properties of Ge with the durability and low cost of Si wafers. However, the 4.2% lattice mismatch between Si and Ge precludes the direct epitaxial growth of defect free and high-quality relaxed Ge layers on top of Si wafers. Efforts to overcome this difficulty are still ongoing in Ge-related research [50–52]. Well-established epitaxial growth techniques and popular for research purposes like solid-source molecular beam epitaxy (SS-MBE), ultra-high vacuum chemical vapour deposition (UHV-CVD) and low-energy plasma-enhanced chemical vapour deposition (LEPE-CVD) are used to grow relaxed Ge buffers on Si. However, in contrast, reduced pressure-chemical vapour deposition (RP-CVD), which is an industrial production technique for modern Si and SiGe device structures, is capable of producing some of the best relaxed and/or slightly tensile strained Ge epilayers on Si substrate. Indeed, relaxed Ge epilayers with thickness below 1 μm on Si(001) exhibits very smooth surface with RMS surface roughness below 1 nm and TDD below 10^7 cm^{-2} [51, 53]. A cross-sectional transmission electron microscopy (XTEM) image showing a typical structure of such epitaxial Ge on Si is shown in Fig. 6.

5 Spin properties of strained Ge While the existence of the Rashba S–O interaction in Ge has been

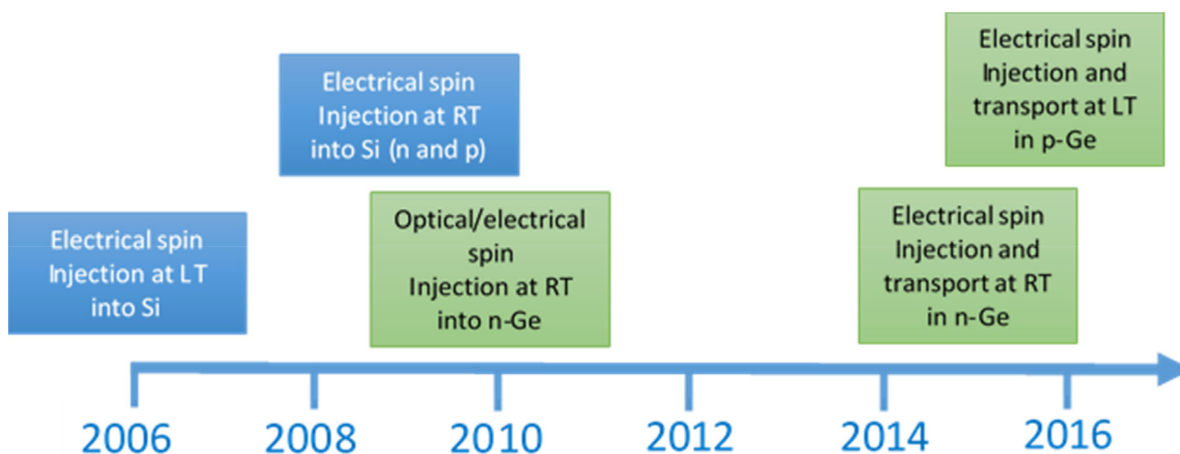

Figure 5 Timeline illustrating key milestones in the progression of the field of group-IV semiconductor spintronics. Achievements are listed for low temperature (~10 K) (LT) and room temperature (RT) techniques.

© 2016 WILEY-VCH Verlag GmbH & Co. KGaA, Weinheim

Table 2 The largest spin lifetimes and spin diffusion lengths measured in Ge at low- and room-temperature. Spin lifetimes determined by three terminal (3T) Hanle and non-local (4T) Hanle are listed.

temperature (K)	dopant type	spin lifetime (3T Hanle) (ns) [14, 45, 46]	spin lifetime (4T Hanle) (ns) [32]	spin diffusion length (3T Hanle) (nm) [14, 47]	spin diffusion length (4T Hanle) (nm) [15, 32]
4	n	0.035	1.08		580
4	p	0.03		30	
300	n	0.5		1500	660

Table 3 Basic electrical and material properties of Si and Ge. Both materials have an indirect (I) band gap.

	Si	Ge
μ_e (cm^2 V^{-1}s^{-1})	1450	3900
$m^*{}_e$ (m$_0$)	1.08	0.55
μ_h (cm^2 V^{-1}s^{-1})	480	1900
$m^*{}_h$ (m$_0$)	$m^*{}_{hh} = 0.49$ $m^*{}_{lh} = 0.16$	$m^*{}_{hh} = 0.28$ $m^*{}_{lh} = 0.044$
E_G (eV)	1.12 (I)	0.66 (I)
ρ (g cm^{-3})	2.3296	5.3234
Mohs hardness	7.0	6.0

known for many years, and evidence was detected using cyclotron resonance techniques [54, 55], it is only recently that the strength of the interaction has been quantified. Also, the interaction in strained Ge QW has been identified as the cubic Rashba S–O interaction, due to quantum confinement in the heavy hole valence band only [56, 57] The energy term arising from the Rashba interaction is cubic in *k*-space, and must be treated with a different analysis to the linear interaction in electron and light hole QW. The S–O interaction is an important component in future spintronic technologies, with applications in areas as diverse as spin transistors, quantum computing (S–O qubits), S–O torque, the spin Hall effect, chiral magnonics and to create band inversion for the formation of topologically insulating states to generate the quantum spin Hall effect [58]. The ubiquitous nature of this physical phenomena has led to the introduction of a new field of research, spin-orbitronics. Beyond these more applied areas of research, the S–O interaction is important in more fundamental areas of research such as cold atom systems, Dirac materials and Majorana fermions.

Figure 7 shows schematics of typical Ge QW heterostructures exhibiting the Rashba S–O interaction. The following is a summary of the key recent findings in this area, focusing on detection and quantification using three methods: analysis of 'beating' patterns in Shubnikov-de Haas (SdH) oscillations [57, 59], analysis of weak anti-localisation (WAL) [56, 59, 60] and cyclotron resonance using terahertz excitation [61]. One of the key advances necessary to observe the Rashba S–O interaction using SdH oscillations is the significant enhancement of 2D hole mobility at low temperatures. Recently, hole mobilities in excess of 1,300,000 cm^2 V^{-1}s^{-1} were achieved in strained Ge QW heterostructures [16, 62–64], with effective masses as low as 0.035 m_0 [65] comparable to the electron effective mass in certain III–V compound semiconductors and to the light hole mass in bulk Ge. The first observation of the cubic Rashba interaction in a Ge QW utilised a SiGe heterostructure containing a 2DHG in a pure Ge, with a low temperature mobility of 450,000 cm^2 V^{-1}s^{-1} [57]. While only less than half of the record 2DHG mobility value, this indicates that the diffusive scattering factors are sufficiently

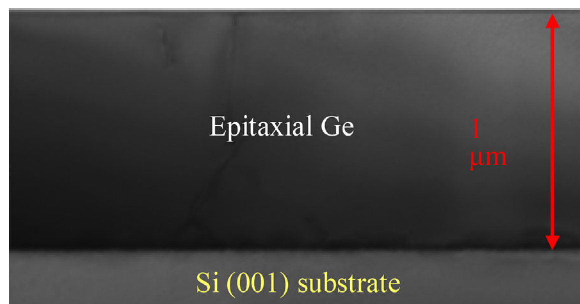

Figure 6 XTEM image showing the typical structure of epitaxial 1 µm thick Ge on Si.

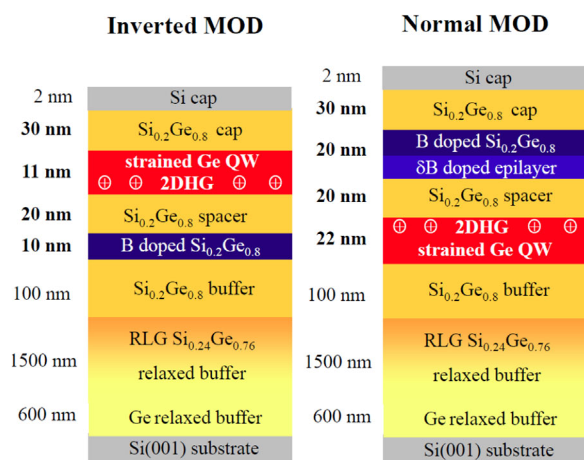

Figure 7 Typical schematics of strained Ge QW heterostructures. From Morrison et al. [59].

© 2016 WILEY-VCH Verlag GmbH & Co. KGaA, Weinheim

low to permit observation of beating effects in SdH oscillations at experimentally accessible magnetic fields. The heterostructure was grown by RP-CVD, the Ge QW grown onto a $Si_{0.2}Ge_{0.8}$ buffer resulting in biaxial compressive strain of 0.8% arising from lattice mismatch. This strain modifies the local band structure of the Ge QW, resulting in a built in potential that modifies the Rashba energy term of the heavy holes. The structural quality of these Ge QW heterostructures is very high. Typical XTEM and AFM images of the heterostructures are shown in Fig. 8.

Most of the defects are localised in the relaxed Ge and SiGe buffer layers. The TDD in the Ge QW near the surface is in the range of $10^6\,cm^{-2}$.

A typical Hall bar device, shown in Fig. 9, was used to measure the magnetoresistance of the Ge QW heterostructures. Magnetotransport measurements at temperatures from 0.4 to 2 K revealed a clear beating pattern in the SdH oscillations, shown in Fig. 10. This arises from the presence of two carrier sub-bands with opposite spin, split in energy by the Rashba interaction illustrated in Fig. 11. SdH oscillations of Rashba spin-split holes may be described by the following equation,

$$\frac{\Delta\rho_{xx}(B)}{\rho_{xx}(0)} = 4\cos\left(\frac{2\pi m^*\left(E_F \pm \beta_{SO}k_F^3\right)}{\hbar eB}\right) \exp\left(-\frac{\pi m^* \alpha_D}{eB\tau_t}\right)\frac{\psi}{\sinh(\psi)}, \qquad (1)$$

where E_F is the Fermi energy, α_D is the Dingle ratio $\left(\frac{\tau_t}{\tau_q}\right)$, where τ_t is the transport scattering time and τ_q is the quantum scattering time, β_{SO} is the cubic Rashba

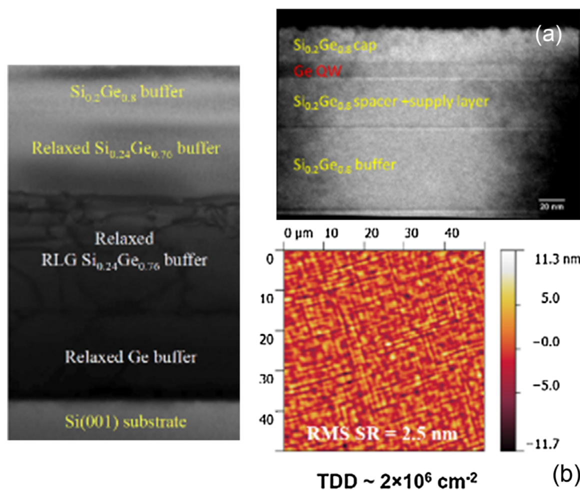

Figure 8 Typical (a) XTEM and (b) AFM of strained Ge QW heterostructures. The XTEM image shows the QW region and the reverse linearly graded (RLG) buffer upon which the electrically active structure is grown. The AFM image shows the RMS surface roughness (SR) and the threading dislocation density (TDD).

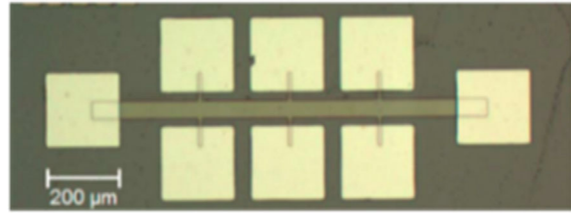

Figure 9 Example optical microscope image of a Hall bar device used for magnetotransport measurements at low temperatures.

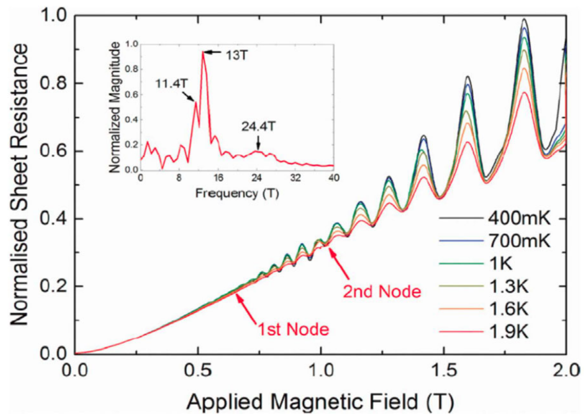

Figure 10 Beating pattern in the Shubnikov de Haas oscilla-tions due to the cubic Rashba spin–orbit interaction. Inset: fast Fourier transform of the oscillations. From Morrison et al. [57].

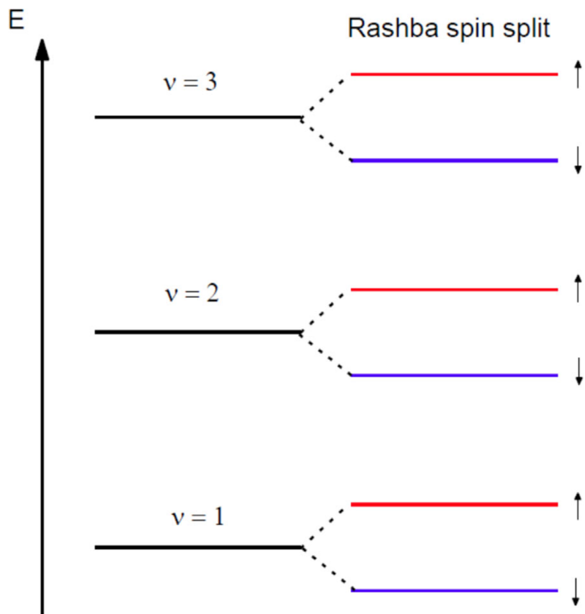

Figure 11 Schematic illustrating the spin-split energy levels created by the Rashba spin–orbit interaction. From Morrison et al. [57].

© 2016 WILEY-VCH Verlag GmbH & Co. KGaA, Weinheim

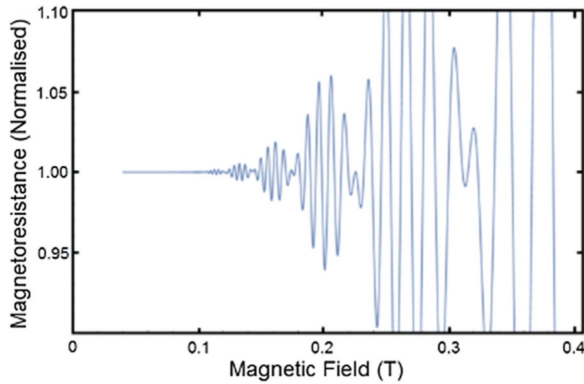

Figure 12 Simulated beating pattern in Shubnikov-de Haas oscillations, due to the Rashba spin–orbit interaction. From Morrison et al. [59].

spin–orbit parameter and

$$\psi = \frac{2\pi^2 k_B T m^*}{\hbar e B}. \tag{2}$$

A simulated plot of Eq. (1) using two spin split carrier bands with a typical splitting energy for a Ge QW is shown in Fig. 12. By performing a fast Fourier transform of the oscillations (Fig. 10, inset), the carrier density of the two sub-bands was determined. The Rashba interaction is cubic in k-space for heavy holes, which are the only carrier type here due to the effect of strain on the band structure, and so the following equation may be used [2]

$$\beta_{SO} = \sqrt{\frac{2}{\pi}} \frac{\hbar^2}{2m^*} \frac{p(p_+ - p_-) + \Delta p(p_+ + p_-)}{6p^2 + 2\Delta p^2}, \tag{3}$$

where $p_\pm = \sqrt{p \pm \Delta p}$, Δp is the difference between the spin up and spin down sub-band hole densities and p is the sum of the spin up and down hole densities. The corresponding spin splitting energy is $2\beta_{SO}k_F^3$.

From Eq. (3), the cubic Rashba coefficient (1×10^{-28} eVm^3) and the spin splitting energy (1.4 meV) were calculated. These values compare favourably to those found in III–V 2D electron gas (2DEG) and 2DHG heterostructures previously characterised, and a more rigorous comparison may be found elsewhere [57]. The values for experimentally determined cubic Rashba coefficients and spin splitting energies in Ge by the methods reviewed here are presented in Table 4. A brief comparison of these values to III–V heterostructures and to Si is given in Table 5. In particular, the Rashba S–O energy of the 2DHG in a Ge QW is the same order of magnitude as ones observed for 2DEG in III–V QWs, which makes Ge more attractive for potential applications. An additional advantage is that the Ge QW is grown on a standard Si(001) substrate by an industrial type RP-CVD process. Comparing to 2DEG in Si QW the Rashba S–O energy of the 2DHG in the Ge QW is three orders of magnitude larger, which again confirms the enormous advantages afforded by Ge.

Among the quantum phenomena that are affected by the Rashba interaction, weak anti-localisation (WAL) is perhaps the most easily observed, occurring at modest magnetic fields and more easily observed in low mobility materials where the transport scattering length is short. WAL is a correction to weak localisation arising from the SOI, and in Ge this is the cubic Rashba interaction. Weak anti-localisation is a quantum correction to the resistivity arising from the interference of coherent partial electron waves forming closed loops, resulting in an increase in the resistance. Upon application of a magnetic field this correction is suppressed, resulting in a characteristic peak at zero magnetic field. The Rashba interaction provides an additional phase difference, resulting in a suppression of weak localisation as the coherence of the closed loops is destroyed. When WAL is dominant, a positive magnetoresistance is observed at low magnetic fields.

To date, measurement of WAL has been used in two Ge QW systems, grown by different techniques, to quantify the cubic Rashba interaction [56, 60]. Firstly, Moriya et al. studied a Ge QW grown by SS-MBE on a $Si_{0.5}Ge_{0.5}$ buffer, resulting in a high degree of biaxial compressive strain (2.1%), and with a low heavy hole mobility in the 2DHG (5000 cm^2 V^{-1}s^{-1}) at low temperatures [56]. By fitting magnetoconductivity data to the Iordanskii–Lyanda-Geller–Pikus model they determined a cubic Rashba coefficient of 1.5×10^{-29} eVm^3, with a corresponding spin splitting energy of 0.36 meV, at zero gate

Table 4 Cubic Rashba spin–orbit parameters and associated energy as determined by analysis of Shubnikov de-Haas oscillations (SdH), weak anti-localisation (WAL) and by THz cyclotron resonance (THz CR). Also included are other important parameters such as the doping profile, the quantum well (QW) thickness, the degree of strain and the heavy hole effective mass.

technique	doping profile	QW thickness (nm)	biaxial compressive strain (%)	cubic Rashba spin–orbit parameter (eVm^3)	Rashba spin–orbit energy (meV)	heavy hole effective mass (m_0)
SdH	inverse	11	0.8	1×10^{-28}	1.4	0.095
THz CR	inverse	11	0.8	9×10^{-29}	2.8	0.103
WAL	normal	22	0.8	–	–	0.065
THz CR	normal	22	0.8	1.2×10^{-28}	0.6	0.087
WAL	normal	20	2.1	1.5×10^{-29}	0.36	0.09

© 2016 WILEY-VCH Verlag GmbH & Co. KGaA, Weinheim

Table 5 Comparison of linear and cubic Rashba interaction parameters in various III–V quantum well systems, in Ge and in Si.

	AlGaN/GaN 2DEG (L) [66]	GaSb/InAs 2DEG (L) [67, 68]	InGaAs/InAlAs 2DEG(L) [69]	Ge 2DHG (C) [57]	Ge 2DHG (C) [56]	Si 2DEG (L) [70]
low temperature mobility ($cm^2 V^{-1} s^{-1}$)	–	~20,000	95,000	450,000	~5000	200,000
Rashba spin–orbit parameter α or β	8.1×10^{-12} eVm	9×10^{-12} eVm	4×10^{-12} eVm	1.0×10^{-28} eVm^3	0.2×10^{-28} eVm^3	5.5×10^{-15} eVm
Rashba spin–orbit energy (meV)	11.6	4	2.5	1.4	0.3	~0.001
lattice mismatch strain	–	–	–	0.80%	2.10%	–

bias. The interaction could be enhanced/suppressed by applying a bias electric field using an electrostatic gate.

A more complex system was studied by Foronda et al., with a high low temperature mobility 2DHG (780000 $cm^2 V^{-1} s^{-1}$) in a Ge QW with a modulation delta dopant layer of boron in proximity [60]. The structures were grown by RP-CVD. Despite this high mobility, and the correspondingly low transport scattering length, a positive magnetoresistance, attributable to WAL, was observed in magnetotransport measurements of this material (Fig. 13). SdH oscillations in the higher field regime are shown in Fig. 14. No evidence was observed of beating in the oscillations, however, it was possible to extract the cubic Rashba parameter for this structure through a THz cyclotron resonance technique [61]. The variety of techniques summarised here, and the failure of some of the techniques for certain material parameters highlights the necessity of employing a multi-technique approach to characterising the SOI in these and other materials.

6 Outlook for future strained Ge spin devices

The spin field-effect transistor envisioned by Datta and Das opened a gateway to spin information processing [5]. Unfortunately, even 26 years later a functional spin field effect transistor for information processing has not been demonstrated yet, although the coherent manipulation of electron spins in semiconductors is now possible. A few fundamental challenges such as the low spin-injection efficiency due to resistance mismatch, spin relaxation and the spread of spin precession angles prevents it. Many alternative spin transistor designs have, therefore, been proposed. But they differ from the original field-effect transistor concept and require the use of optical or magnetic elements. As a consequence, it creates serious obstacles for implementation of such devices into modern ultra large scale integrated circuits. Proposed designs for a spin-valve/4 terminal Hanle device and a spin transistor incorporating a Ge QW are presented in Fig. 15. The current/voltage configuration indicated in the top part of Fig. 15 is for Hanle measurements of spin transport in the Ge QW to determine the spin diffusion length. The middle two (ferromagnetic contacts) may be used as the source and drain for spin valve operation – shape anisotropy of the

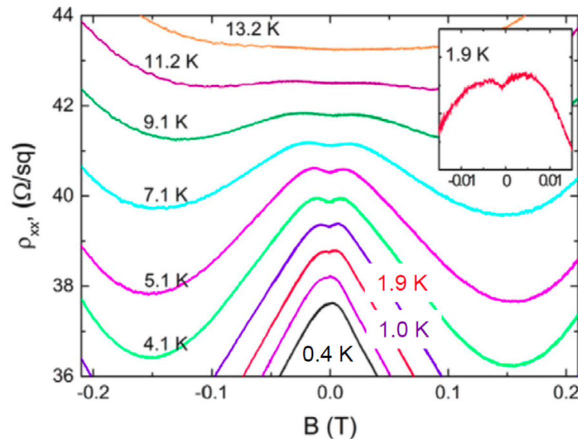

Figure 13 Evolution of the low field magnetoresistance from positive (WAL) to negative (WL) with temperature. From Foronda et al. [60].

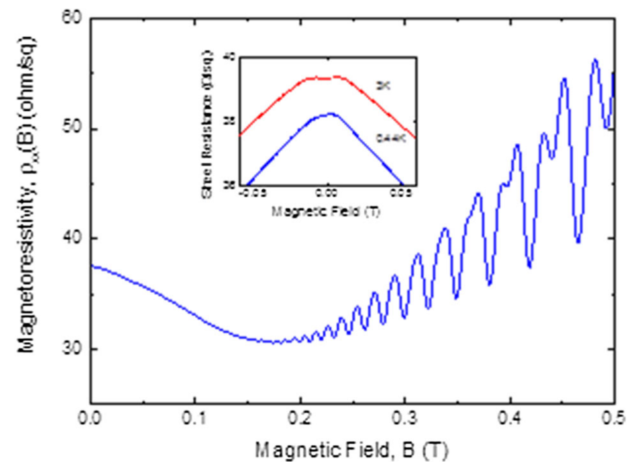

Figure 14 Low field magnetoresistance at 0.3 K for the normal modulation doped 22 nm Ge quantum well showing the onset of Zeeman splitting. Inset: Evidence of weak anti-localisation effects near zero field.

© 2016 WILEY-VCH Verlag GmbH & Co. KGaA, Weinheim

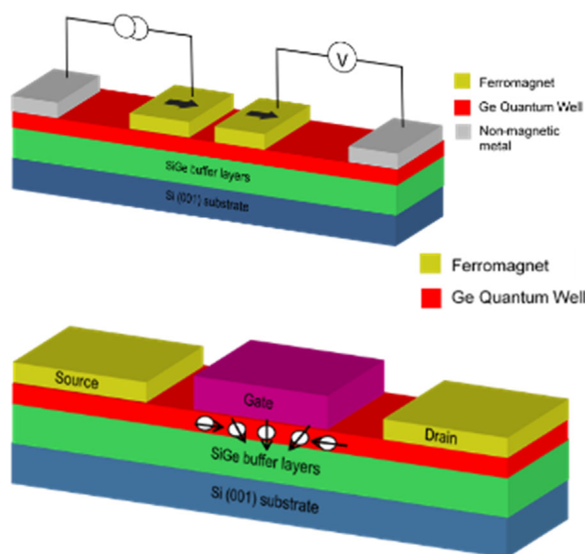

Figure 15 (Top) Layout of proposed four terminal Ge quantum well spin device for non-local Hanle and spin valve measurements. (Bottom) Spin FET proposal utilising a Ge quantum well as the channel.

contacts (different sizes) allows switching of one contact in a magnetic field while the other remains fixed. The bottom figure shows a proposed spin FET design utilising a Ge QW as the channel. This is intended to operate in the same fashion as the spin FET outlined earlier, as originally proposed by Datta and Das.

The high quality SiGe-relaxed buffer is essential for epitaxial growth of the compressive strained Ge QW. Only four monolayers of strained Ge can be grown on a Si(001) substrate. This thickness is insufficient for formation of a quantised level in the Ge QW and consequently appearance of the 2DHG. The effect of compressive strain in the Ge QW on spin transport properties has yet to be confirmed experimentally, but the Ge QWs described above are suitable for fabrication of Hanle and then SpinFET devices. However, the major obstacles appear to come from selection of suitable ferromagnetic contact materials, dielectric interfacial layer and the techniques used to for their deposition or growth. The quality of the materials and interfaces as well as their reproducibility are essential to obtain working spin devices. The smallest lateral dimensions in these devices ought to be well below 1 μm, which requires nanoscale e-beam lithography for prototyping them in research labs.

Alternatively, an all-electric and all-semiconductor spin field-effect transistor in which these obstacles are overcome could be realised in low-dimensional Ge structures by using two quantum point contacts as spin injectors and detectors. The first demonstration of such device has recently been demonstrated using III–V epitaxial structures [71]. But in the case of Ge, an even more advanced device architecture can be implemented. For an example, the devices could be realised via fabrication of quantum wire etched of epitaxial Ge and surrounded by GeO_2 as a natural choice or another

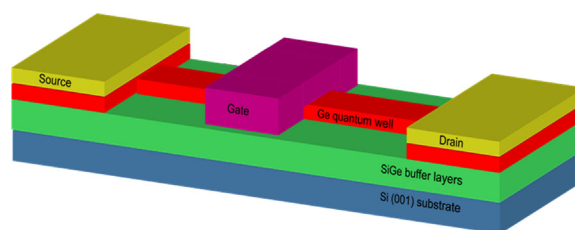

Figure 16 Proposal for a spin polarising device utilising 1D confinement of holes in a Ge nanowire.

gate dielectric and a metal contact deposited on top, or patterning the Ge surface with split gate devices with sub 100 nm dimensions. Figure 16 shows the device's layout. In both cases, e-beam lithography is essential to pattern nm scale features. The 1D confining potential in a strained Ge QW creates a structure where the spin-polarisation of an applied current is fundamental without applied magnetic fields, DC voltage bias, electrical spin-injection or optical pumping. Distinct engineering architectures of spin–orbit coupling could be exploited for the quantum point contacts and the central semiconductor channel to achieve complete control of the electron spins (spin injection, manipulation and detection) in a purely electrical manner. Such a device is compatible with large-scale integration and holds promise for future spintronic devices for information processing.

7 Summary Germanium (Ge) is another Group IV semiconductor material, which recently started attracting tremendous attention in spintronics following success of Si. The first experimental demonstration of room-temperature spin transport in heavily doped epitaxial Ge has recently been reported. Strained Ge QW heterostructures offer many promising opportunities for advancing our knowledge of spin interactions and producing spintronic devices. It has been shown that the Rashba SOI in strained Ge QW heterostructures can be identified and quantified using two complimentary low temperature magnetotransport techniques – weak anti-localisation and SdH oscillation frequency analysis as well as two methods using THz cyclotron resonance spectroscopy. SOI-based effects, strong in Ge, allow us to exploit new methods for controlling spin transport and for spin injection/extraction. An outlook has been presented for the future of strained Ge spin devices including several example designs.

References

[1] R. Jansen, Nature Mater. **11**, 400 (2012).
[2] R. Winkler, Spin–Orbit Coupling Effects in Two-Dimensional Electron and Hole Systems (Springer, Berlin, Heidelberg, New York, 2003).
[3] M. D'yakonov, Spin Physics in Semiconductors (Springer, Berlin, Heidelberg, New York, 2008).
[4] A. B. Yu and E. I. Rashba, J. Phys. C **17**, 6039 (1984).
[5] S. Datta and B. Das, Appl. Phys. Lett. **56**, 665 (1990).

 © 2016 WILEY-VCH Verlag GmbH & Co. KGaA, Weinheim

[6] E. Y. Tsymbal and I. Žutić, Handbook of Spin Transport and Magnetism (CRC, Boca Raton, 2011).
[7] B. C. Min, K. Motohashi, C. Lodder, and R. Jansen, Nature Mater. **5**, 817 (2006).
[8] S. P. Dash, S. Sharma, R. S. Patel, M. P. de Jong, and R. Jansen, Nature **462**, 491 (2009).
[9] C. H. Li, O. M. van't Erve, and B. T. Jonker, Nature Commun. **2**, 245 (2011).
[10] T. Suzuki, T. Sasaki, T. Oikawa, M. Shiraishi, Y. Suzuki, and K. Noguchi, Appl. Phys. Express **4**, 023003 (2011).
[11] J. H. Pifer, Phys. Rev. B **12**, 4391 (1975).
[12] Y. Ochiai and E. Matsuura, Phys. Status Solidi A **38**, 243 (1976).
[13] V. Zarifis and T. G. Castner, Phys. Rev. B **57**, 14600 (1998).
[14] A. Jain, J. C. Rojas-Sanchez, M. Cubukcu, J. Peiro, J. C. Le Breton, E. Prestat, C. Vergnaud, L. Louahadj, C. Portemont, C. Ducruet, V. Baltz, A. Barski, P. Bayle-Guillemaud, L. Vila, J. P. Attane, E. Augendre, G. Desfonds, S. Gambarelli, H. Jaffres, J. M. George, and M. Jamet, Phys. Rev. Lett. **109**, 106603 (2012).
[15] S. Dushenko, M. Koike, Y. Ando, T. Shinjo, M. Myronov, and M. Shiraishi, Phys. Rev. Lett **114**, 196602 (2015).
[16] A. Dobbie, M. Myronov, R. J. H. Morris, a. H. a. Hassan, M. J. Prest, V. a. Shah, E. H. C. Parker, T. E. Whall, and D. R. Leadley, Appl. Phys. Lett. **101**, 172108 (2012).
[17] M. Myronov, C. Morrison, J. Halpin, S. Rhead, C. Casteleiro, J. Foronda, V. A. Shah, and D. Leadley, Jpn. J. Appl. Phys. **53**, 04EH02 (2014).
[18] M. Myronov, C. Morrison, J. Halpin, S. Rhead, J. Foronda, and D. Leadley, Solid-State Electron. **110**, 35 (2015).
[19] K. Morii, T. Iwasaki, R. Nakane, M. Takenaka, and S. Takagi, IEEE Electron Device Lett. **31**, 1092 (2010).
[20] G. Feher and A. F. Kip, Phys. Rev. **97**, 337 (1955).
[21] D. K. Wilson, Phys. Rev. **134**, A265 (1964).
[22] R. E. Pontinen and T. M. Sanders, Phys. Rev. **152**, 850 (1966).
[23] E. M. Gershenzon, N. M. Pevin, and M. S. Fogelson, Phys. Status Solidi B **49**, 411 (1972).
[24] A. I. Veinger, A. G. Zabrodskii, T. V. Tisnek, and S. I. Goloshchapov, Semiconductors **42**, 1274 (2009).
[25] A. I. Veĭnger, A. G. Zabrodskiĭ, T. V. Tisnek, and S. I. Goloshchapov, Semiconductors **41**, 790 (2007).
[26] C. Hautmann, B. Surrer, and M. Betz, Phys. Rev. B **83**, 161203 (2011).
[27] C. Guite and V. Venkataraman, Phys. Rev. Lett. **107**, 166603 (2011).
[28] E. J. Loren, J. Rioux, C. Lange, J. E. Sipe, H. M. van Driel, and A. L. Smirl, Phys. Rev. B **84**, 214307 (2011).
[29] F. Pezzoli, F. Bottegoni, D. Trivedi, F. Ciccacci, A. Giorgioni, P. Li, S. Cecchi, E. Grilli, Y. Song, M. Guzzi, H. Dery, and G. Isella, Phys. Rev. Lett. **108**, 156603 (2012).
[30] K. Kenji, F. Yuichi, Y. Shinya, S. Kentarou, M. Masanobu, and H. Kohei, Appl. Phys. Express **7**, 033002 (2014).
[31] L. T. Chang, W. Han, Y. Zhou, J. Tang, I. A. Fischer, M. Oehme, J. Schulze, R. K. Kawakami, and K. L. Wang, Semicond. Sci. Technol. **28**, 015018 (2013).
[32] Y. Zhou, W. Han, L.-T. Chang, F. Xiu, M. Wang, M. Oehme, I. A. Fischer, J. Schulze, R. K. Kawakami, and K. L. Wang, Phys. Rev. B **84**, 125323 (2011).
[33] C. Shen, T. Trypiniotis, K. Y. Lee, S. N. Holmes, R. Mansell, M. Husain, V. Shah, X. V. Li, H. Kurebayashi, I. Farrer, C. H. d. Groot, D. R. Leadley, G. Bell, E. H. C. Parker, T. Whall, D. A. Ritchie, and C. H. W. Barnes, Appl. Phys. Lett. **97**, 162104 (2010).
[34] A. T. Hanbicki, S. F. Cheng, R. Goswami, O. M. J. van't Erve, and B. T. Jonker, Solid State Commun. **152**, 244 (2012).
[35] K.-R. Jeon, B.-C. Min, Y.-H. Jo, H.-S. Lee, I.-J. Shin, C.-Y. Park, S.-Y. Park, and S.-C. Shin, Phys. Rev. B **84**, 165315 (2011).
[36] Y. Aoki, M. Kameno, Y. Ando, E. Shikoh, Y. Suzuki, T. Shinjo, M. Shiraishi, T. Sasaki, T. Oikawa, and T. Suzuki, Phys. Rev. B **86**, 081201 (2012).
[37] T. Uemura, K. Kondo, J. Fujisawa, K.-I. Matsuda, and M. Yamamoto, Appl. Phys. Lett. **101**, 132411 (2012).
[38] O. Txoperena, Y. Song, L. Qing, M. Gobbi, L. E. Hueso, H. Dery, and F. Casanova, Phys. Rev. Lett. **113**, 146601 (2014).
[39] Y. Song and H. Dery, Phys. Rev. Lett. **113**, 047205 (2014).
[40] O. Txoperena, M. Gobbi, A. Bedoya-Pinto, F. Golmar, X. Sun, L. E. Hueso, and F. Casanova, Appl. Phys. Lett. **102**, 192406 (2013).
[41] H. N. Tinkey, P. Li, and I. Appelbaum, Appl. Phys. Lett. **104**, 232410 (2014).
[42] A. G. Swartz, S. Harashima, Y. Xie, D. Lu, B. Kim, C. Bell, Y. Hikita, and H. Y. Hwang, Appl. Phys. Lett. **105**, 032406 (2014).
[43] A. Tsukahara, Y. Ando, Y. Kitamura, H. Emoto, E. Shikoh, M. P. Delmo, T. Shinjo, and M. Shiraishi, Phys. Rev. B **89**, 235317 (2014).
[44] C. Lin, I. Shoji, M. Fumihiro, and O. Hideo, Appl. Phys. Express **7**, 013002 (2014).
[45] A. Jain, L. Louahadj, J. Peiro, J. C. Le Breton, C. Vergnaud, A. Barski, C. Beigné, L. Notin, A. Marty, V. Baltz, S. Auffret, E. Augendre, H. Jaffrès, J. M. George, and M. Jamet, Appl. Phys. Lett. **99**, 162102 (2011).
[46] H. Saito, S. Watanabe, Y. Mineno, S. Sharma, R. Jansen, S. Yuasa, and K. Ando, Solid State Commun. **151**, 1159 (2011).
[47] F. Rortais, S. Oyarzun, F. Bottegoni, J. C. Rojas-Sanchez, P. Laczkowski, A. Ferrari, C. Vergnaud, C. Ducruet, C. Beigne, N. Reyren, A. Marty, J. P. Attane, L. Vila, S. Gambarelli, J. Widiez, F. Ciccacci, H. Jaffres, J. M. George, and M. Jamet, J. Phys.: Condens. Matter **28**, 165801 (2016).
[48] C. Rinaldi, M. Cantoni, D. Petti, A. Sottocorno, M. Leone, N. M. Caffrey, S. Sanvito, and R. Bertacco, Adv. Mater. **24**, 3037 (2012).
[49] F. Bottegoni, A. Ferrari, S. Cecchi, M. Finazzi, F. Ciccacci, and G. Isella, Appl. Phys. Lett. **102**, 152411 (2013).
[50] D. Choi, Y. Ge, J. S. Harris, J. Cagnon, and S. Stemmer, J. Cryst. Growth **310**, 4273 (2008).
[51] V. A. Shah, A. Dobbie, M. Myronov, and D. R. Leadley, Thin Solid Films **519**, 7911 (2011).
[52] Y. Yamamoto, P. Zaumseil, T. Arguirov, M. Kittler, and B. Tillack, Solid-State Electron. **60**, 2 (2011).
[53] V. A. Shah, A. Dobbie, M. Myronov, and D. R. Leadley, Solid-State Electron. **62**, 189 (2011).
[54] C. M. Engelhardt, D. Többen, M. Aschauer, F. Schäffler, G. Abstreiter, and E. Gornik, Solid-State Electron. **37**, 949 (1994).
[55] R. Winkler, M. Merkler, T. Darnhofer, and U. Rössler, Phys. Rev. B **53**, 10858 (1996).
[56] R. Moriya, K. Sawano, Y. Hoshi, S. Masubuchi, Y. Shiraki, A. Wild, C. Neumann, G. Abstreiter, D. Bougeard, T. Koga, and T. Machida, Phys. Rev. Lett **113**, 086601 (2014).

© 2016 WILEY-VCH Verlag GmbH & Co. KGaA, Weinheim

[57] C. Morrison, P. Wiśniewski, S. D. Rhead, J. Foronda, D. R. Leadley, and M. Myronov, Appl. Phys. Lett. **105**, 182401 (2014).
[58] A. Manchon, H. C. Koo, J. Nitta, S. M. Frolov, and R. A. Duine, Nature Mater. **14**, 871 (2015).
[59] C. Morrison, J. Foronda, P. Wiśniewski, S. D. Rhead, D. R. Leadley, and M. Myronov, Thin Solid Films **602**, 84 (2016).
[60] J. Foronda, C. Morrison, J. E. Halpin, S. D. Rhead, and M. Myronov, J. Phys.: Condens. Matter **27**, 022201 (2014).
[61] M. Failla, M. Myronov, C. Morrison, D. R. Leadley, and J. Lloyd-Hughes, Phys. Rev. B **92**, 045303 (2015).
[62] Q. Shi, M. A. Zudov, C. Morrison, and M. Myronov, Phys. Rev. B **91**, 241303 (2015).
[63] Q. Shi, M. A. Zudov, C. Morrison, and M. Myronov, Phys. Rev. B **92**, 161405 (2015).
[64] Q. Shi, M. A. Zudov, C. Morrison, and M. Myronov, Phys. Rev. B **91**, 201301 (2015).
[65] C. Morrison, and M. Myronov, Phys. Rev. Lett. (submitted) (2016).
[66] K. S. Cho, T.-Y. Huang, H.-S. Wang, M.-G. Lin, T.-M. Chen, C. T. Liang, Y. F. Chen, and I. Lo, Appl. Phys. Lett. **86**, 222102 (2005).
[67] J. Luo, H. Munekata, F. F. Fang, and P. J. Stiles, Phys. Rev. B **38**, 10142 (1988).
[68] J. Luo, H. Munekata, F. F. Fang, and P. J. Stiles, Phys. Rev. B **41**, 7685 (1990).
[69] B. Das, D. C. Miller, S. Datta, R. Reifenberger, W. P. Hong, P. K. Bhattacharya, J. Singh, and M. Jaffe, Phys. Rev. B **39**, 1411 (1989).
[70] Z. Wilamowski, W. Jantsch, H. Malissa, and U. Rössler, Phys. Rev. B **66**, 195315 (2002).
[71] P. Chuang, S. C. Ho, L. W. Smith, F. Sfigakis, M. Pepper, C. H. Chen, J. C. Fan, J. P. Griffiths, I. Farrer, H. E. Beere, G. A. Jones, D. A. Ritchie, and T. M. Chen, Nature Nanotechnol. **10**, 35 (2015).

 © 2016 WILEY-VCH Verlag GmbH & Co. KGaA, Weinheim